IOP Publishing J. Phys. Energy 5 (2023) 044002 https://doi.org/10.1088/2515-7655/acf957

Journal of Physics: Energy

CrossMark

OPEN ACCESS

RECEIVED
16 February 2023

REVISED
27 July 2023

ACCEPTED FOR PUBLICATION
13 September 2023

PUBLISHED
25 September 2023

PAPER

Entropy change reversibility in $MnNi_{1-x}Co_xGe_{0.97}Al_{0.03}$ near the triple point

Tapas Samanta[1,*], **Chris Taake**[1], **Laila Bondzio**[1] **and Luana Caron**[1,2]

[1] Faculty of Physics, Bielefeld University, PO Box 100131, Bielefeld D-33501, Germany
[2] Helmholtz-Zentrum Berlin für Materialien und Energie, Berlin 12489, Germany
[*] Author to whom any correspondence should be addressed.

E-mail: tapas.sinp@gmail.com and tsamanta@physik.uni-bielefeld.de

Keywords: magnetocaloric effect, triple point, reversible entropy change, lattice softening

Supplementary material for this article is available online

Abstract

The nature of the phase transition has been studied in $MnNi_{1-x}Co_xGe_{0.97}Al_{0.03}$ ($x = 0.20$–0.50) through magnetization, differential scanning calorimetry and x-ray diffraction measurements; and the associated reversibility in the magnetocaloric effect has been examined. A small amount of Al substitution for Ge can lower the structural phase transition temperature, resulting in a coupled first-order magnetostructural transition (MST) from a ferromagnetic orthorhombic to a paramagnetic hexagonal phase in $MnNi_{1-x}Co_xGe_{0.97}Al_{0.03}$. Interestingly, a composition-dependent triple point (TP) has been detected in the studied system, where the first-order MST is split into an additional phase boundary at higher temperature with a second-order transition character. The critical-field-value of the field-induced MST decreases with increasing Co concentration and disappears at the TP ($x = 0.37$) resembling most field-sensitive MST among the studied compositions. An increase of the hexagonal lattice parameter a_{hex} near the TP indicates a lattice softening associated with an enhancement of the vibrational amplitude in the Ni/Co site. The lattice softening leads to a larger field-induced structural entropy change (structural entropy change$\gg$ magnetic entropy change, for this class of materials) with the application of a lower field, which results in a larger reversibility of the low-field entropy change ($|\Delta S_{rev}| = 6.9$ J kg^{-1} K for $\Delta\mu_0 H = 2$ T) at the TP.

1. Introduction

Phase transitions in magnetic materials always draw special attention of the scientific community due to the fascinating fundamental insights they provide while being the origin of different application-oriented functional properties, such as magnetoresistance [1], magnetic shape memory [2], barocaloric [3] and magnetocaloric effects (MCEs) [4]. Among the wide variety of magnetic phase transitions and their delicate balance, they are broadly classified into two categories, namely second-order (SOMT) and first-order (FOMT) magnetic phase transitions. The nature of phase transitions is relatively well explored for materials exhibiting a pure SOMT from a ferromagnetic (FM) to a paramagnetic (PM) state. The discontinuous variation of the order parameter associated with the FOMT makes it rather complicated to explain the phase transition considering a well-defined representation. Still, a consistent effort has been dedicated to explore magnetic materials exhibiting a FOMT due to their enhanced functional properties in comparison to those presenting SOMTs.

The magnetostructural (magnetostructural transition (MST)) or magnetoelastic FOMT between an ordered FM to a disordered PM state acquired surplus attention because of their attractive multifunctional properties associated with large magnetization jumps [3–9]. It has also been extensively studied that the FOMT between two ordered states can give rise to large magnetization changes and result in large multifunctional properties [1, 2, 10]. However, the unavoidable thermal hysteresis associated with FOMT often limits the reversibility of these functional properties. There are several intrinsic (e.g. nature of magnetic

ordering, spin fluctuations) and extrinsic (e.g. microstructure) components of the observed hysteresis associated with the FOMT [11]. Often it is hard to determine their origin and which component is dominant. Many different routes have been applied in order to reduce the thermal hysteresis and to improve the reversibility of functional properties. The improvement of the structural compatibility at MSTs is one of the most prominent [12].

In this context, let us imagine a hypothetical scenario where thermal hysteresis remains almost invariant upon compositional variation. Could it still be possible to further improve the functional properties' reversibility? To get more insight, a systematic study of phase transitions has been conducted in $MnNi_{1-x}Co_xGe_{0.97}Al_{0.03}$ compounds and the reversibility of the MCE, in terms of the isothermal entropy change (ΔS) has been examined. The determination of this system's phase diagram revealed a composition-dependent triple point (TP) due to the separation of a single MST line into SOMT and FOMT boundaries. An improvement of the low-field reversible entropy change $|\Delta S_{rev}|$ has been observed near the TP and the possible origin of the effect has been discussed.

Stoichiometric MnNiGe and MnCoGe compounds exhibit antiferromagnetic (AFM) with a spiral magnetic structure and FM ordered states below their respective SOMT temperatures, Néel temperature T_N ($\sim$346 K) [13] and Curie temperature T_C ($\sim$345 K) [14]. A structural transition between a low-temperature TiNiSi-type orthorhombic to a high-temperature Ni_2In-type hexagonal structure occurs in the PM state. Therefore, increasing the substitution of Co for Ni in $MnNi_{1-x}Co_xGe$ can weaken the AFM order and stabilize a higher magnetization state (such as FM, ferrimagnetic, FM spiral) with a magnetic instability near 50:50 substitutions, as reported in the literature [15, 16]. The previously generated phase diagram also indicates that the magnetic and structural transitions remain decoupled in $MnNi_{1-x}Co_xGe$, while only the nature of magnetic ordering changes [15, 17]. Although, Ren *et al* reported a coupled MST in the intermediate composition range of $Mn(Co_{1-x}Ni_x)Ge$, this could be related with the different sample preparation and annealing procedure [18]. A hydrostatic-pressure-induced TP has also been previously reported for the studied class of materials [16, 19]. However, the composition-dependent TP is not well studied and deserves more attention, especially in view of related functional properties. Pressure-induced TPs are very interesting from a fundamental point of view. However, a composition-dependent TP is more relevant for applications. Moreover, the comparison of the materials' properties around pressure-induced and composition-dependent TPs can yield interesting information on the nature of the MST. To investigate the composition-dependent TP, we selected the $MnNi_{1-x}Co_xGe_{0.97}Al_{0.03}$ system for our study. In addition to the already described characteristics, in this system the substitution of a small amount of Al for Ge results in a coupled MST even for higher Ni-concentration due to the decrease of the structural transition temperature. A similar effect on the structural stability and realization of the MST has been observed earlier for the Al-substituted MnNiGe system [20, 21] and it is also consistent with the proposed stabilization of the hexagonal phase in MnNiGe by isostructural substitution of MnNiAl through DFT calculation [22].

2. Experimental methods

All polycrystalline $MnNi_{1-x}Co_xGe_{0.97}Al_{0.03}$ ($x = 0.20$–0.50) samples were prepared by arc melting of the constituent elements of purity better than 99.9% in an argon atmosphere. To compensate the weight loss due to the high vapor pressure of Mn, 2 wt% extra Mn was added during melting for all the studied samples. The as-cast samples were further sealed inside a pre-evacuated partially argon-filled quartz tube and annealed at 900 °C for 2 d followed by furnace cooling. To determine the crystal structure, room-temperature x-ray diffraction (XRD) measurements were carried out on a Philips X'Pert Pro MPD diffractometer using Cu K_α radiation. An XPERT-PRO diffractometer with Cu K_α radiation source and a TTK-450 low temperature chamber were used for the temperature-dependent XRD measurements. Structural refinement of the XRD data was executed using the FullProf software to estimate the lattice parameters [23]. The chemical compositions of selected samples have been estimated using elemental analysis in FEI Helios NanoLab 600i DualBeam Focused Ion Beam with EDAX addon. The scan area of the measurement was about 1 mm^2. The results are summarized in the supplementary material. The magnetization measurements were performed using a Quantum Design MPMS 3 magnetometer for the temperature interval of 5–360 K with applied magnetic fields up to $\mu_0 H = 7$ T. High-temperature (up to 950 K) magnetization measurements were carried out using the oven option of the MPMS 3 magnetometer. In order to avoid artifacts in the estimation of the ΔS of a FOMT [24], isofield $M(T)$ data have been used for calculations using the Maxwell relation:

$$\Delta S\ (T,\ \mu_0 H) = \sum_i \frac{M_{i+1}\,(T_{i+1},\ \mu_0 H) - M_i\,(T_i,\ \mu_0 H)}{T_{i+1} - T_i}\ \Delta\mu_0 H,$$

where M_{i+1} (T_{i+1}, $\mu_0 H$) and M_i (T_i, $\mu_0 H$) represent the values of magnetization in a magnetic field $\mu_0 H$ at temperatures T_{i+1} and T_i, respectively. The reversible $|\Delta S_{rev}|$ is the effective entropy change excluding the unavoidable thermal hysteresis loss due to the FOMT, which can be exploited for a cyclic magnetic cooling application and is estimated as the overlap of the temperature-dependent entropy change curves on heating and cooling [25]. Differential scanning calorimetry (DSC) measurements were executed using a DSC25 (TA Instruments) with a temperature sweep rate of 10 K min^{-1} during heating and cooling.

3. Results and discussion

From the room temperature XRD measurements, it has been found that all the compositions crystalize in a hexagonal Ni_2In-type crystal structure. Rietveld refinements of the XRD data for all studied compositions are included in the supplementary material. The composition-dependent variation of the hexagonal lattice parameters (c_{hex} and a_{hex}) is shown in figure 1(a). A decrease of c_{hex} has been observed with increasing x with a significant change between the $x = 0.35$ and 0.40 compositions. A peak-like feature has been detected in the variation of a_{hex} within the composition range $0.30 \leqslant x \leqslant 0.40$, exhibiting a maximum at $x = 0.37$. Significantly larger vibrational amplitude for Co atoms along a_{hex} has been identified earlier for the MnCoGe system in its hexagonal Ni_2In-type crystal structure [26]. Therefore, the observed increase in a_{hex} for $x = 0.30$–0.37 is associated with an enhancement of the vibrational amplitude in the Ni/Co site. In turn, the composition-dependent increase of a_{hex} results in an increase of the hexagonal unit cell volume (V_{hex}) (as shown in figure 1(b)) and, consequently, makes the hexagonal lattice softer (indicating that a transformation from a high-temperature hexagonal to a low-temperature orthorhombic martensitic phase is easier upon external perturbation) [26]. The plot of $c_{hex}/a_{hex}(x)$ is shown in figure 1(c). Similar to $c_{hex}(x)$, the c_{hex}/a_{hex} ratio decreases with increasing x with a slightly larger variation in between the compositions $x = 0.35$ and 0.37. Temperature-dependent XRD measurements were carried out to identify the low-temperature crystal structure for the compositions $x = 0.30$, 0.37 and 0.40. The XRD patterns as measured at different constant temperatures for $x = 0.30$, 0.37 and 0.40 are shown in figures 2(a)–(c), respectively. At low-temperature a TiNiSi-type orthorhombic phase has been detected similar to that observed in this class of material [21]. The orthorhombic lattice parameters at 100 K were found to be $a_{orth} = 6.014(3)$, 6.005(1), 5.996(3) Å, $b_{orth} = 3.754(1)$, 3.752(1), 3.755(2) Å and $c_{orth} = 7.089(3)$, 7.086(1), 7.074(3) Å for $x = 0.30$, 0.37, 0.40, respectively. Rietveld refinements profiles at 100 K can be found in the supplementary material.

The composition-dependent variation of magnetization (M) as a function of temperature (T) is shown in figure 3(a) for a $\mu_0 H = 0.1$ T applied magnetic field. The thermal hysteresis between heating and cooling $M(T)$ curves indicates the first-order nature of the phase transition, which is associated with a MST from a low-temperature TiNiSi-type orthorhombic to a high-temperature Ni_2In-type hexagonal phase. Moreover, an increase of M in the low-temperature phase due to the MST signifies that the FOMT occurs between a FM orthorhombic to a PM (or lower magnetization state) hexagonal phase. The FOMT was also detected in the DSC heat flow curve (shown in figure 3(b)) as evident from the clearly visible endothermic/exothermic peaks during heating/cooling and thermal hysteresis. The latent heat (L) as estimated from the DSC heat flow curve decreases monotonically with increasing x and then a saturation tendency has been observed for $x \geqslant 0.4$, as shown in figure 3(c) (right axis) for heating. However, the variation of the total transition entropy change ($\Delta S_{tr} = L/T_M$, where T_M is transition temperature corresponding to the MST) as a function of x shows a clear change near the composition $x = 0.37$ (figure 3(c) (left axis)).

The composition-dependent magnetic phase diagram as depicted in figure 3(d) was generated using $M(T)$ curves measured applying a $\mu_0 H = 0.1$ T magnetic field. A single spiral-FM to PM MST has been observed for $x \leqslant 0.37$ [27]. The orthorhombic FM state transforms to an AFM-like state at temperatures below the MST for all the studied compositions, which is consistent with the literature for similar materials classes [15, 17, 18, 28]. For $x > 0.37$, the single MST splits into two transitions: one second-order in character followed by a FOMT at lower temperature. In this case, the SOMT starts during cooling, but is not complete: the partial magnetic transition is completed through the coincidence with the structural transition (T_{st}) in a cooperative manner if T_{st} falls at the edge (or intermediate region) of the magnetic transition [29, 30]. The overlap of the second-order FM transition (T_C) line with the first-order MST phase boundary results in a 'triple point' (TP) for $x = 0.37$. A similar type of TP was previously reported induced by hydrostatic pressure [16, 19] and sometimes observed in elemental substituted MnTX (T=Co, Ni and X=Ge, Si) systems [29, 30].

Magnetic field ($\mu_0 H$) dependent magnetization data has been collected for all studied compositions in the close vicinity of their respective phase transition temperatures (FM to PM MST), T_M, during heating as shown in figure 4(a) (see left axis). A magnetic-field-induced MST has been detected for $x \leqslant 0.35$. The critical field value ($\mu_0 H_C$) of the field-induced MST has been estimated by considering the maximum value of $dM/d(\mu_0 H)$ as plotted in figure 4(a) (see right axis). The variation of $\mu_0 H_C(x)$ is shown in figure 4(b).

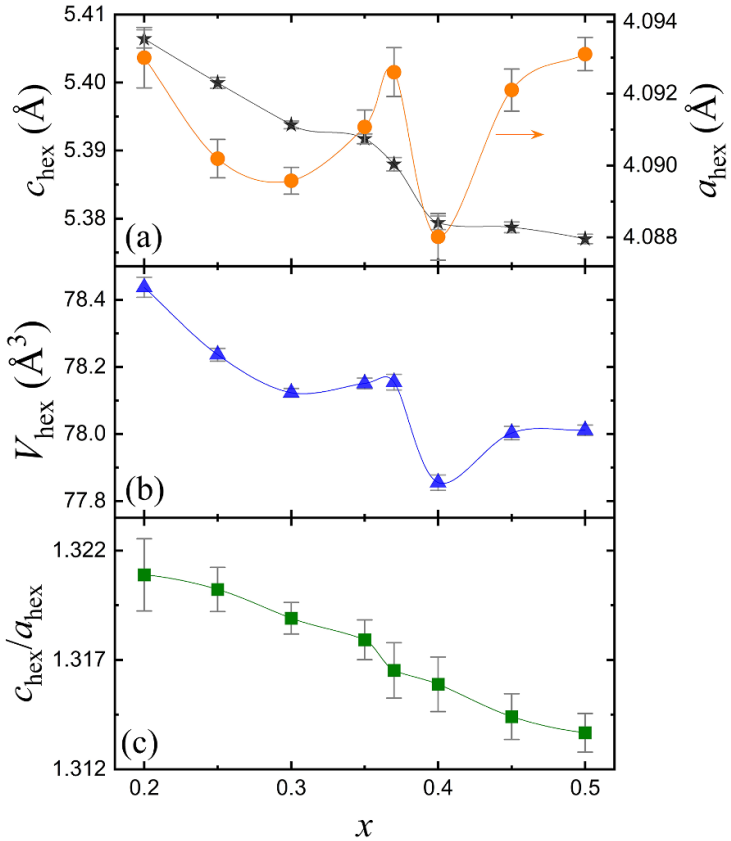

Figure 1. (a) The variation of hexagonal lattice parameters (c_{hex} and a_{hex}) at room-temperature as a function of composition (x) in $MnNi_{1-x}Co_xGe_{0.97}Al_{0.03}$. (b) Change of hexagonal unit cell volume V_{hex} with composition. (c) The composition-dependent modification of the ratio c_{hex}/a_{hex} is plotted.

$\mu_0 H_C$ decreases almost linearly with increasing x and disappears at $x = 0.37$ indicating a better field-sensitivity of the magnetic-field-induced MST near the TP.

To examine the composition-dependent variation of the saturation magnetization (M_S), isothermal magnetization measurements as a function of $\mu_0 H$ were carried out at 5 K, these are plotted in figure 5(a). A field-induced metamagnetic transition from an AFM-like state to a FM state has been observed in the low-temperature orthorhombic state, which is more pronounced for lower x. The critical field value of the metamagnetic transition decreases with increasing x and almost disappears for $x = 0.50$, indicating a progressive destabilization of the AFM state with increasing Co-concentration. The temperature-dependent variation of the inverse susceptibility ($1/\chi$) for $\mu_0 H = 0.1$ T in the hexagonal PM state is shown in figure 5(b) for the $x = 0.37$ and 0.40 compositions (the details of the $1/\chi(T)$ plot for all compositions are included in the supplementary material), which is used to estimate the effective magnetic moment (μ_{eff}) in the PM state. A modified Curie-Weiss expression, $\chi = \chi_0 + C/(T\text{-}\theta_P)$ was employed to fit the $1/\chi(T)$ data, where C, θ_P and χ_0 are the Curie constant, PM Curie temperature and T-independent susceptibility, respectively [31]. From the fitting, the values of C and θ_P have been evaluated. The variation of the μ_{eff} (as estimated from C) as a function of x is illustrated in figure 5(c) (right axis) and qualitatively compared with $M_S(x)$. A sharp increase in M_S has been observed for a slight variation in composition from $x = 0.37$–0.40 near the TP, however, μ_{eff} decreases suddenly in the same compositional range. $|\Delta S|(T)$ curves during heating and cooling are shown in figure 6(b) for $x = 0.37$ with $\Delta\mu_0 H = 2$ T as a representing figure for evaluating the reversible entropy change $|\Delta S_{rev}|$. The details of the variation in $\Delta S(T)$ and concomitant $|\Delta S_{rev}|$ up to $\mu_0 H = 7$ T for all studied compositions can be found in the supplementary material. The composition-dependent variation in $|\Delta S_{rev}|$ as a function of $\mu_0 H$ is plotted in figure 6(c). A change of curvature in $|\Delta S_{rev}|(\mu_0 H)$ for lower x is a characteristic feature of a field-induced MST, which disappears at the TP. With the application of a magnetic field $\mu_0 H > \mu_0 H_C$, a relatively faster increase (nearly linear) in $|\Delta S_{rev}|$ has been observed for $x \leqslant 0.3$, which is consistent with the observed larger total transition entropy change ΔS_{tr} of the respective composition (see figure 3(c)). As a result, a large $|\Delta S_{rev}|$ of 17.2 J kg^{-1} K (24.5) for $\Delta\mu_0 H = 5$ T (7) has been observed for $x = 0.30$, which is comparable with the largest reversible reported value in this class of materials ($|\Delta S_{rev}| = 18.6$ J kg^{-1} K for $\Delta\mu_0 H = 5$ T) as well as other well-known giant magnetocaloric materials [12].

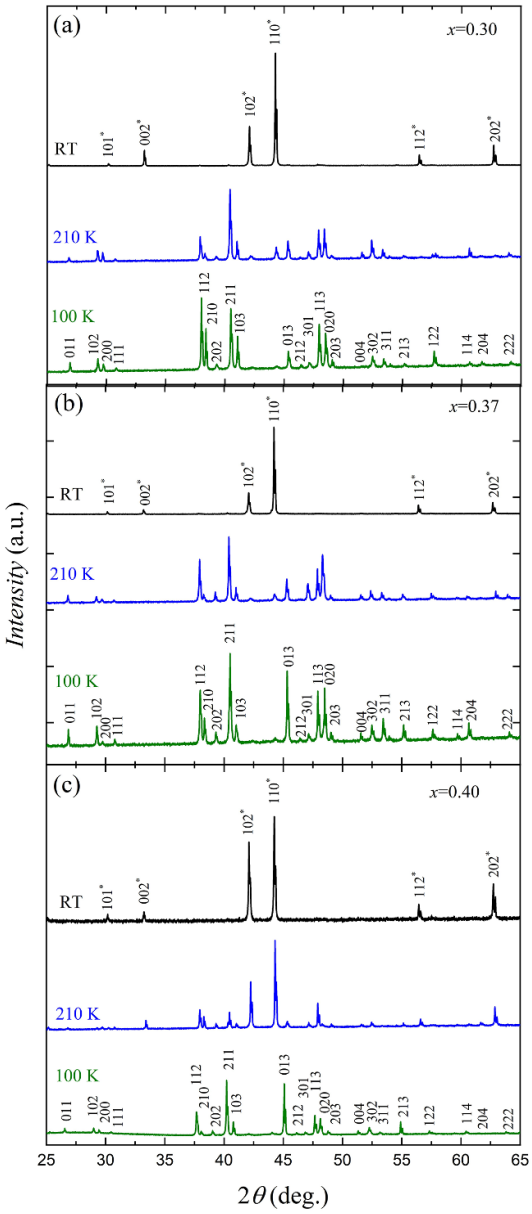

Figure 2. Temperature-dependent XRD patterns for $MnNi_{1-x}Co_xGe_{0.97}Al_{0.03}$ with (a) $x = 0.30$, (b) $x = 0.37$ and (c) $x = 0.40$, respectively. The Miller indices of the hexagonal and orthorhombic phases are indicated with and without an asterisk, respectively.

The variation of $|\Delta S_{rev}|$ under high-field is a valuable information to gain more insight about the nature of the phase transition. Moreover, a large $|\Delta S_{rev}|$ at fields up to 2 T is desirable for applications such as magnetic cooling, since it can be achieved using a permanent magnet. The composition-dependent variation of $|\Delta S_{rev}|$ for $\Delta\mu_0 H = 2$ T is shown in figure 6(d). Interestingly, $|\Delta S_{rev}|$ reaches a maximum value ($|\Delta S_{rev}| = 6.9$ J kg^{-1} K for $\Delta\mu_0 H = 2$ T) at the TP ($x = 0.37$). The observed $|\Delta S_{rev}|$ for $\Delta\mu_0 H \leqslant 2$ T is large for this class of materials (e.g. $|\Delta S_{rev}| = 2$ and 1.9 J kg^{-1} K for $\Delta\mu_0 H = 1$ T in $Mn_{1-x}Fe_{2x}Ni_{1-x}Ge$ [12], $MnNi_{1-x}Co_xGe$ [17], respectively, which is 3.6 J kg^{-1} K for the same field change in case of the presently studied system) and is comparable to that of Gd [32] and NiMn-based Heusler alloys [10]. However, the value is moderate in comparison to other well-known giant magnetocaloric materials, such as Fe_2P-based and $La(Fe_{1-x}Si_x)_{13}$ compounds [33]. The major focus in the present study is not just to report the absolute value of the reversible $|\Delta S_{rev}|$, rather to understand the origin of the enhanced reversibility near the TP; these are discussed as follows.

The representative diagram of the variations of the entropy change (ΔS) as a function of temperature in the presence of magnetic field up to 7 T for $x = 0.37$ in the vicinity of MST is shown in figure 6(a) for heating and cooling, respectively. A large direct MCE has been observed, which is associated with a MST between a low-temperature FM TiNiSi-type orthorhombic to a high-temperature PM Ni_2In-type hexagonal phase. An

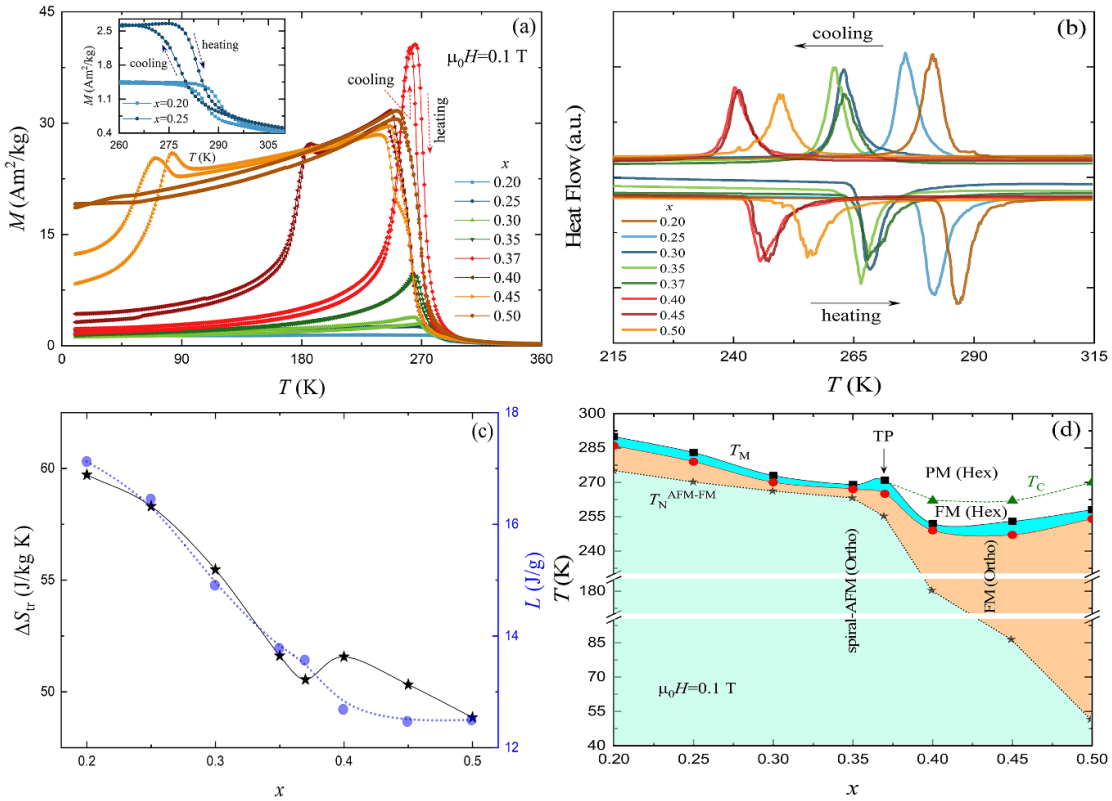

Figure 3. (a) Temperature dependence of the magnetization (M) during heating and cooling for $MnNi_{1-x}Co_xGe_{0.97}Al_{0.03}$ in the presence of magnetic fields $\mu_0H = 0.1$ T. Inset: plot of M(T) in the close vicinity of MST for $x = 0.20$ and 0.25. (b) DSC heat flow curves as a function of temperature during heating and cooling for $MnNi_{1-x}Co_xGe_{0.97}Al_{0.03}$. (c) (left axis) Transition entropy (ΔS_{tr}) and (right axis) latent heat (L) are plotted as a function of x for heating. (d) The magnetic phase diagram as generated using M(T) data measured in the presence of $\mu_0H = 0.1$ T. The triple point (TP) as detected for the composition $x = 0.37$ is indicated by the arrow.

inverse MCE has also been detected due to the spiral-AFM to FM transition near T_N^{AFM-FM} (as shown in the insets of figure 6(a)), similar to that observed in earlier studies [17, 18].

Two types of dependence in T_M have been reported for the MnTX system: a nearly linear variation with (*i*) valence electron concentration (*e*/*a*) [34–37] or (*ii*) a_{orth}/b_{orth} ratio ($\equiv c_{hex}/a_{hex}$) [12, 37]. The substitution of small elements or application of hydrostatic pressure usually results in a decrease of c_{hex}/a_{hex} and also a reduction of T_M associated with the stabilization of the high-temperature hexagonal phase at lower temperature [37–40]. The stabilization of the hexagonal phase can also be accomplished by substituting bigger elements with fewer valence electrons [18, 20, 21, 41]. In this case, a more complicated dependence of T_M has been observed, which is associated with a competition between the variation of the *e*/*a* ratio and chemical pressure (as generated due to the modification of the local environment by substituting different size elements). The situation is similar in the present studied $MnNi_{1-x}Co_xGe_{0.97}Al_{0.03}$ system. Partial substitution of the bigger elements Al and Co (with fewer valence electrons than Ge and Ni, respectively) for smaller Ge and Ni, respectively, results in a coupled MST in $MnNi_{1-x}Co_xGe_{0.97}Al_{0.03}$. A small primary Al substitution for Ge can establish a coupled MST in Ni-rich $MnNi_{1-x}Co_xGe_{0.97}Al_{0.03}$ as observed earlier for Al and In-substituted MnNiGe systems [20, 21, 41, 42]. With increasing Co-concentration, T_M initially decreases with decreasing *e*/*a* ratio. With further increase of Co-concentration ($x \geqslant 0.3$), the chemical pressure (as generated by the substitution of bigger Co for smaller Ni) starts to compete with the variation in *e*/*a* to modify the T_M. As a result, a deviation from the linear dependence of T_M with *e*/*a* has been observed ($x \geqslant 0.37$). The negative chemical pressure starts to expand the hexagonal unit cell for $x > 0.3$ and reaches a maximum value at the TP ($x = 0.37$). The increase of V_{hex} is associated with an increase of the hexagonal lattice parameter a_{hex} (however, a progressive decrease is accounted for by c_{hex}) due to the enhancement of the vibrational amplitude in the Ni/Co site [26], which results in a lattice softening near the TP.

After crossing the TP for $x = 0.4$, an abrupt contraction of V_{hex} associated with the decrease of both a_{hex} and c_{hex} generates a positive chemical pressure and decreases T_M due to the stabilization of the low-volume hexagonal phase. The effect of chemical pressure likely has a lower impact on the magnetic transition temperature, T_C, in agreement with the effect of pure hydrostatic pressure [16]. As a result, the T_C remains

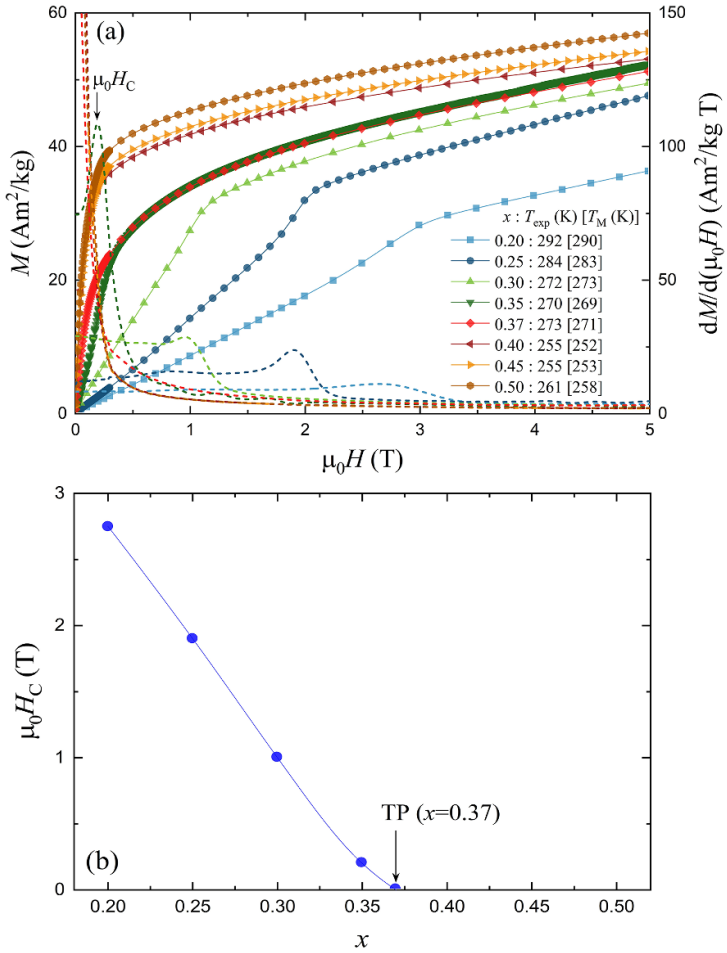

Figure 4. (a) Magnetization isotherms as a function of magnetic field (shown by solid symbols as connected with lines) near MST of the respective composition, x (left axis). Plot of dM/d($\mu_0 H$) (shown by dashed lines), as used to determine the critical field value ($\mu_0 H_C$) of field-induced MST (right axis). (d) $\mu_0 H_C$ as a function of x. Field-induced MST disappears at TP ($x = 0.37$). Solid line through the data points is a guide to the eye.

almost unchanged, only T_M moves to lower temperature. Eventually, the splitting of T_C and T_M results in a TP at $x = 0.37$. A similar TP has been observed earlier for related systems with the application of hydrostatic pressure [16, 19]. The TP has been also realized in the elemental-substituted MnCoGe system [21, 30, 38, 43] and the existence of the effect has been explained as a result of the reduction in the magnetostructural coupling constant [43]. A pronounced increase of M_S for $x > 0.37$ likely excludes the possibility of band hybridization, which can stabilize a non-collinear magnetic structure by modifying the electronic density of states at the Fermi level. However, based on the sudden reduction of μ_{eff} in the PM state, a slight variation of the electronic state cannot be ignored for the composition with $x = 0.4$. The modification of the electronic state could improve the bond strength at the expense of magnetism by the formation of a non-collinear magnetic state [18]. A similar type of competition between magnetism and bonding has been observed in $Mn(Co_{1-x}Ni_x)Ge$ by Ren *et al* [18] and is considered as the driving force of the FOMT in transition metal Fe_2P-based giant magnetocaloric materials [44].

For a MST, there are two entropy contributions, namely structural entropy change $|\Delta S_{st}|$ and magnetic entropy change $|\Delta S_M|$, to the total isothermal entropy change $|\Delta S|$ [45]. The addition of $|\Delta S_{st}|$ and $|\Delta S_M|$ results in a total $|\Delta S|$ as $|\Delta S| = |\Delta S_{st}| + |\Delta S_M|$ for the MnTX system [45]. Usually, a much larger $|\Delta S_{st}|$ has been observed in the MnTX system when compared to $|\Delta S_M|$ due to a large volume change at the MST resulting in $|\Delta S| \sim |\Delta S_{st}|$ [46, 47]. Therefore, a large $|\Delta S|$ can be realized for a large change in $|\Delta S_{st}|$. The lattice softening due to the enhancement of the vibrational amplitude in the Ni/Co site along a_{hex} (which favor the low-temperature orthorhombic martensitic phase) and a better field-sensitivity of the magnetic-field-induced MST near the TP (as shown in figure 4(a)), make it easier to transform a larger FM orthorhombic martensitic phase fraction with the application of a lower magnetic field in comparison to the other compositions and result in a better low-field reversibility in $|\Delta S_{rev}|$. Above the TP ($x \geqslant 0.4$), the decrease of the low-field $|\Delta S_{rev}|$ could be related with the reduction in the magnetostructural coupling

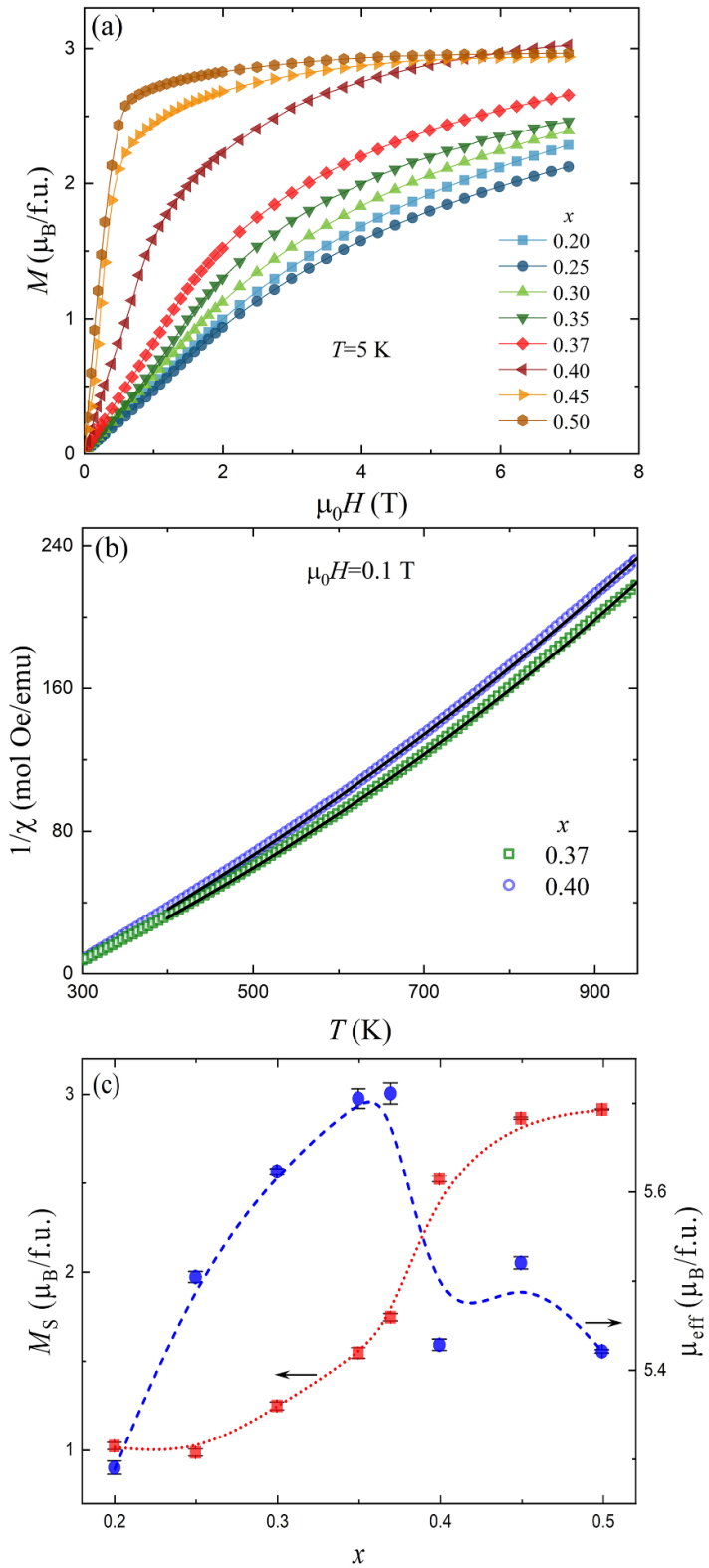

Figure 5. (a) Field-dependent magnetization as measured at 5 K. (b) Plot of inverse susceptibility ($1/\chi$) as a function of temperature in the presence of $\mu_0 H = 0.1$ T for the compositions $x = 0.37$ and 0.40. Solid lines through the data points are the corresponding fitting in the temperature interval of 400–950 K. (c) Variations of saturation magnetization (M_S) and effective magnetic moment (μ_{eff}) as a function of composition.

constant similar to that observed earlier [16, 43]. The decrease of the Zeeman energy in the FM martensitic phase (the field-induced MST is incomplete for $x = 0.2$ as $\mu_0 H_C > 2$ T) diminishes the low-field value of $|\Delta S_{rev}|$ (due to a smaller change in ΔM across the MST) with increasing Ni-concentration below the TP.

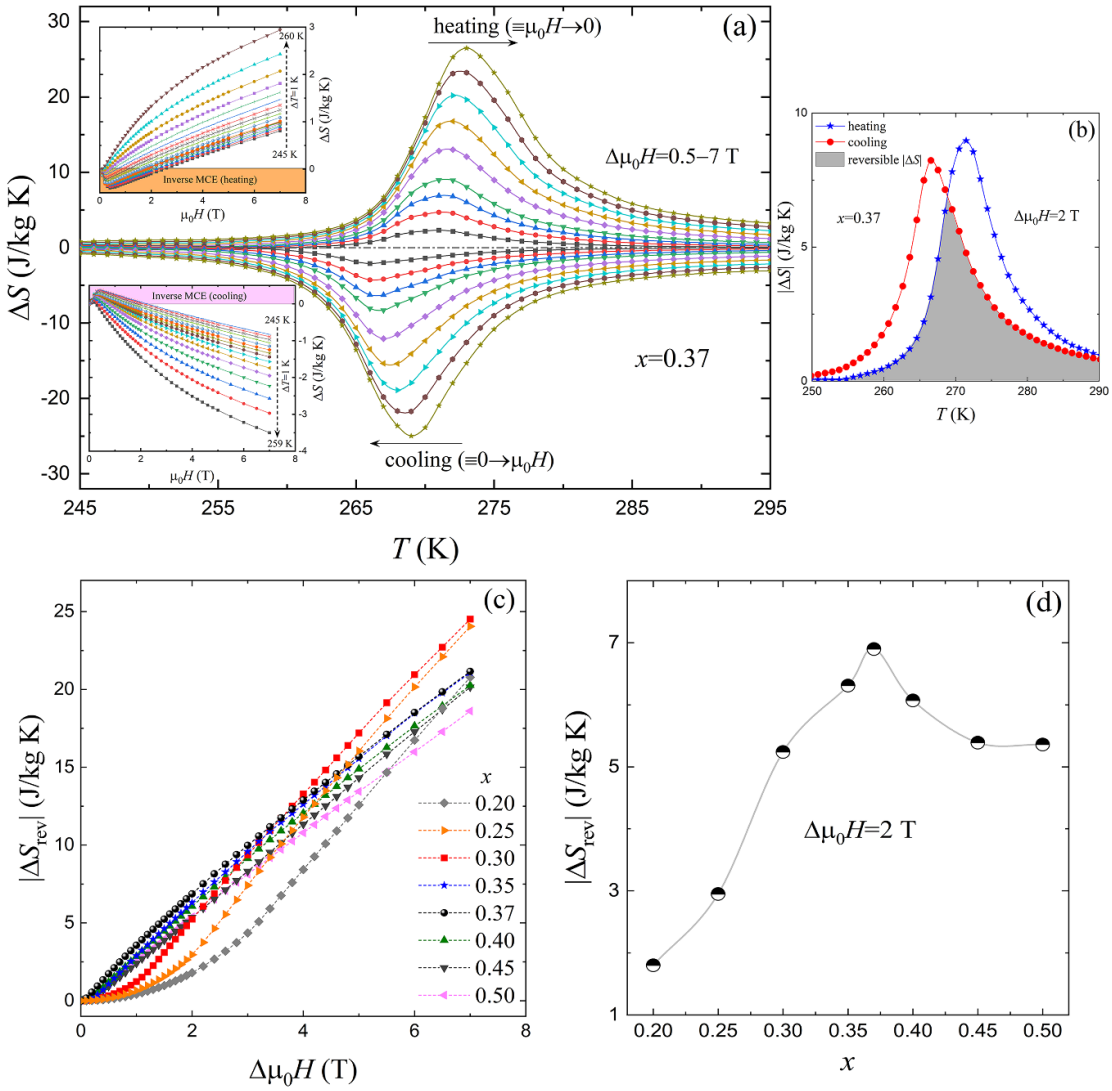

Figure 6. (a) Entropy change (ΔS) as a function of temperature for $x = 0.37$ during heating and cooling with the application of magnetic field ($\mu_0 H$) up to 7 T. Inset: inverse MCE for heating (upper inset) and cooling (lower inset) are shown by $\Delta S(\mu_0 H)$ plots, which is associated with a phase transformation from a spiral-AFM to FM transition near $T_N^{\text{AFM-FM}}$ below the MST. (b) Temperature dependence of $|\Delta S|$ for $x = 0.37$ with a change of magnetic field of $\mu_0 H = 2$ T. The reversible region of ΔS ($|\Delta S_{\text{rev}}|$) is highlighted in gray. (c) The maximum reversible entropy change ($|\Delta S_{\text{rev}}|$) as a function of magnetic field variation up to 7 T for all the studied compositions. (d) Composition dependent $|\Delta S_{\text{rev}}|$ for $\mu_0 H = 2$ T.

4. Conclusions

The substitution of bigger-size elements with fewer valence electrons can establish a coupled MST in the MnNiGe-based system. The stability of the MST and therefore the variation of T_M depends on the delicate balance between the modification of the valence electron concentration e/a and chemical pressure as induced by elemental substitution in $MnNi_{1-x}Co_xGe_{0.97}Al_{0.03}$. The competition of the above-mentioned two factors results in a composition-dependent TP for $x = 0.37$. Interestingly, a better low-field reversibility in $|\Delta S_{\text{rev}}|$ has been observed near the TP. It has been found that the combined effects of lattice softening and a higher field sensitivity of the magnetic-field-induced MST can transform a larger fraction of the FM orthorhombic phase near the TP with the application of a lower field. Consequently, the contribution of ΔS_{st} to ΔS is enhanced at low-field, which leads to a better $|\Delta S_{\text{rev}}|$ near the TP. The present study indicates that the investigation of the magnetocaloric properties near the TP could be of interest for the studied class of materials with an expectation to realize a better reversible entropy change.

Data availability statement

All data that support the findings of this study are included within the article (and any supplementary files).

Acknowledgments

This work was carried out in the framework of the Joint Lab BiBer and was supported by the BMBF joint project DiProMag—Digitalization of a process chain for the production, characterization and prototypical application of magnetocaloric alloys, here the contribution of Bielefeld University: FKZ 13XP5 120B, with the objective of producing magnetocaloric Heusler compounds and ontology development. The authors thank B J R Dankelman (from TUDelft, The Netherlands) for carrying out the temperature-dependent XRD measurements.

ORCID iD

Tapas Samanta https://orcid.org/0000-0002-0964-502X

References

[1] Yu S Y, Liu Z H, Liu G D, Chen J L, Cao Z X, Wu G H, Zhang B and Zhang X X 2006 Large magnetoresistance in single-crystalline $Ni_{50}Mn_{50-x}In_x$ alloys (x=14–16) upon martensitic transformation *Appl. Phys. Lett.* **89** 162503
[2] Kainuma R *et al* 2006 Magnetic-field-induced shape recovery by reverse phase transformation *Nature* **439** 957
[3] Samanta T *et al* 2018 Barocaloric and magnetocaloric effects in $(MnNiSi)_{1-x}(FeCoGe)_x$ *Appl. Phys. Lett.* **112** 021907
[4] Pecharsky V K and Gschneidner J K A Jr 1997 Giant magnetocaloric effect in $Gd_5(Si_2Ge_2)$ *Phys. Rev. Lett.* **78** 4494
[5] Tang H, Pecharsky V K, Samolyuk G D, Zou M, Gschneidner J K A Jr, Antropov V P, Schlagel D L and Lograsso T A 2004 Anisotropy of the magnetoresistance in $Gd_5Si_2Ge_2$ *Phys. Rev. Lett.* **93** 237203
[6] Fujita A, Fujieda S, Hasegawa Y and Fukamichi K 2003 Itinerant-electron metamagnetic transition and large magnetocaloric effects in $La(Fe_xSi_{1-x})_{13}$ compounds and their hydrides *Phys. Rev.* B **67** 104416
[7] Tegus O, Brück E, Buschow K H J and de Boer F R 2002 Transition-metal-based magnetic refrigerants for room-temperature applications *Nature* **415** 150
[8] Stadler S, Khan M, Mitchell J, Ali N, Gomes A M, Dubenko I, Takeuchi A Y and Guimarães A P 2006 Magnetocaloric properties of $Ni_2Mn_{1-x}Cu_xGa$ *Appl. Phys. Lett.* **88** 192511
[9] Wada H and Tanabe Y 2001 Giant magnetocaloric effect of $MnAs_{1-x}Sb_x$ *Appl. Phys. Lett.* **79** 3302
[10] Stern-Taulats E, Castillo-Villa P O, Mañosa L, Frontera C, Pramanick S, Majumdar S and Planes A 2014 Magnetocaloric effect in the low hysteresis Ni-Mn-In metamagnetic shape-memory Heusler alloy *J. Appl. Phys.* **115** 173907
[11] Gutfleisch O *et al* 2016 Mastering hysteresis in magnetocaloric materials *Philos. Trans.* A **374** 20150308
[12] Liu J, Gong Y, You Y, You X, Huang B, Miao X, Xu G, Xu F and Brück E 2019 Giant reversible magnetocaloric effect in MnNiGe-based materials: minimizing thermal hysteresis via crystallographic compatibility modulation *Acta Mater.* **174** 450
[13] Bażela W, Szytuła A, Todorović T, Tomkowicz Z and Zięba A 1976 Crystal and magnetic structure of NiMnGe *Phys. Status Solidi* A **38** 721
[14] Kanomata T, Ishigaki H, Suzuki T, Yoshida H, Abe S and Kaneko T 1995 Magneto-volume effect of $MnCo_{1-x}Ge(0\leqslant x\leqslant 0.2)$ *J. Magn. Magn. Mater.* **140–144** 131
[15] Nizioł S, Bombik A, Bażela W, Szytuła A and Fruchart D 1982 Magnetic phase diagram of $Co_xNi_{1-x}MnGe$ *Solid State Commun.* **42** 79
[16] Nizioł S, Zięba A, Zach R, Baj M and Dmowski L 1983 Structural and magnetic phase transitions in $Co_xNi_{1-x}MnGe$ system under pressure *J. Magn. Magn. Mater.* **38** 205
[17] Zhang C L, Chena J, Wang T Z, Xie G X, Zhua C and Wang D H 2011 The magnetic phase transitions and magnetocaloric effect in $MnNi_{1-x}Co_xGe$ alloys *Solid State Commun.* **151** 1359
[18] Ren Q, Hutchison W D, Wang J, Studer A J and Campbell S J 2018 Magnetic and structural transitions tuned through valence electron concentration in magnetocaloric $Mn(Co_{1-x}Ni_x)Ge$ *Chem. Mater.* **30** 1324
[19] Anzai S and Ozawa K 1978 Coupled nature of magnetic and structural transition in MnNiGe under pressure *Phys. Rev.* B **18** 2173
[20] Samanta T, Dubenko I, Quetz A, Temple S, Standler S and Ali N 2012 Magnetostructural phase transitions and magnetocaloric effects in $MnNiGe_{1-x}Al_x$ *Appl. Phys. Lett.* **100** 052404
[21] Quetz A, Samanta T, Dubenko I, Kangas M J, Chan J Y, Stadler S and Ali N 2013 Phase diagram and magnetocaloric effects in aluminum doped MnNiGe alloys *J. Appl. Phys.* **114** 153909
[22] Fortunato N M, Taubel A, Marmodoro A, Pfeuffer L, Ophale I, Ebert H, Gutfleisch O and Zhang H 2023 High-throughput design of magnetocaloric materials for energy applications: MM´X alloys *Adv. Sci.* **2023** 2206772
[23] Rodríguez-Carvajal J 2015 Introduction to the program FULLPROF: refinement of crystal and magnetic structures from powder and single crystal data (Laboratoire Léon Brillouin, CEA/Saclay)
[24] Caron L, Doan N B and Ranno L 2017 On entropy change measurements around first order phase transitions in caloric materials *J. Phys.: Condens. Matter* **29** 075401
[25] Kaeswurm B, Franco V, Skokov K P and Gutfleisch O 2016 Assessment of the magnetocaloric effect in La, Pr(Fe,Si) under cycling *J. Magn. Magn. Mater.* **406** 259
[26] Jeitschko W 1975 A high-temperature x-ray study of the displacive phase transition in MnCoGe *Acta Crystallogr.* **B31** 1187
[27] Nizioł S, Bombik A, Bazela W, Szytuła A and Fruchart D 1982 Crystal and magnetic structure of $Co_xNi_{1-x}MnGe$ system *J. Magn. Magn. Mater.* **27** 281
[28] Trung N T, Biharie V, Zhang L, Caron L, Buschow K H J and Brück E 2010 From single- to double-first-order magnetic phase transition in magnetocaloric $Mn_{1-x}Cr_xCoGe$ compounds *Appl. Phys. Lett.* **96** 162507
[29] Samanta T, Dubenko I, Quetz A, Stadler S and Ali N 2013 Large magnetocaloric effects due to the coincidence of martensitic transformation with magnetic changes below the second-order magnetic phase transition in $Mn_{1-x}Fe_xCoGe$ *J. Magn. Magn. Mater.* **330** 88
[30] Samanta T, Dubenko I, Quetz A, Stadler S and Ali N 2013 Large magnetocaloric effects over a wide temperature range in $MnCo_{1-x}Zn_xGe$ *J. Appl. Phys.* **113** 17A922

[31] Mugiraneza S and Hallas A M 2022 Tutorial: a beginner's guide to interpreting magnetic susceptibility data with the Curie-Weiss law *Commun. Phys.* **5** 95
[32] Dan'kov S Y, Tishin A M, Pecharsky V K and Gschneidner K A 1998 Magnetic phase transitions and the magnetothermal properties of gadolinium *Phys. Rev.* B **57** 3478
[33] Gottschall T, Skokov K P, Fries M, Taubel A, Radulov I, Scheibel F, Benke D, Riegg S and Gutfleisch O 2019 Making a cool choice: the materials library of magnetic refrigeration *Adv. Energy Mater.* **9** 1901322
[34] Liu E K, Zhu W, Feng L, Chen J L, Wang W H, Wu G H, Liu H Y, Meng F B, Luo H Z and Li Y X 2010 Vacancy-tuned paramagnetic/ferromagnetic martensitic transformation in Mn-poor $Mn_{1-x}CoGe$ alloys *Europhys. Lett.* **91** 17003
[35] Franco V, Blázquez J S, Ipus J J, Law J Y, Moreno-Ramírez L M and Conde A 2018 Magnetocaloric effect: from materials research to refrigeration devices *Prog. Mater. Sci.* **93** 112
[36] Tozkoparan O, Yildirim O, Yüzüak E, Duman E and Dincer I 2019 Magnetostructural transition in Co-Mn-Ge systems tuned by valence electron concentration *J. Alloys Compd.* **791** 208
[37] Song Y *et al* 2020 Magneto-structural coupling through bidirectionally controlling the valence electron concentration in MnCoGe alloy *J. Magn. Magn. Mater.* **495** 165865
[38] Samanta T, Dubenko I, Quetz A, Prestigiacomo J, Adams P W, Stadler S and Ali N 2013 $Mn_{1-x}Fe_xCoGe$: a strongly correlated metal in the proximity of a noncollinear ferromagnetic state *Appl. Phys. Lett.* **103** 042408
[39] Samanta T, Dubenko I, Quetz A, Stadler S and Ali N 2012 Giant magnetocaloric effects near room temperature in $Mn_{1-x}Cu_xCoGe$ *Appl. Phys. Lett.* **101** 242405
[40] Samanta T *et al* 2015 Effects of hydrostatic pressure on magnetostructural transitions and magnetocaloric properties in $(MnNiSi)_{1-x}(FeCoGe)_x$ *J. Appl. Phys.* **117** 123911
[41] Wu R R, Bao L F, Hu F X, Wang J, Zheng X Q, Liu Y, Sun J R and Shen B G 2014 Effect of substitution of In for Co on magnetostructural coupling and magnetocaloric effect in $MnCo_{1-x}In_xGe$ compounds *J. Appl. Phys.* **115** 17A911
[42] Wu R-R *et al* 2015 Giant barocaloric effect in hexagonal Ni_2In-type Mn-Co-Ge-In compounds around room temperature *Sci. Rep.* **5** 18027
[43] Choudhury D, Suzuki T, Tokura Y and Taguchi Y 2014 Tuning structural instability toward enhanced magnetocaloric effect around room temperature in $MnCo_{1-x}Zn_xGe$ *Sci. Rep.* **4** 7544
[44] Boeije M F J, Roy P, Guillou F, Yibole H, Miao X F, Caron L, Banerjee D, van Dijk N H, de Groot R A and Brück E 2016 Efficient room-temperature cooling with magnets *Chem. Mater.* **28** 4901
[45] Gschneidner K A Jr, Mudryka Y and Pecharsky V K 2012 On the nature of the magnetocaloric effect of the first-order magnetostructural transition *Scr. Mater.* **67** 572
[46] Samanta T *et al* 2015 Hydrostatic pressure-induced modifications of structural transitions lead to large enhancements of magnetocaloric effects in MnNiSi-based systems *Phys. Rev.* B **91** 020401(R)
[47] Guillou F, Wilhelm F, Tegus O and Rogalev A 2016 Microscopic mechanism of the giant magnetocaloric effect in MnCoGe alloys probed by x-ray magnetic circular dichroism *Appl. Phys. Lett.* **108** 122405